Produktinformation

Forschungsprodukte & Biochemikalien

Zellkultur & Verbrauchsmaterial

Diagnostik & molekulare Diagnostik

Laborgeräte & Service

Weitere Information auf den folgenden Seiten!
See the following pages for more information!

Lieferung & Zahlungsart

siehe unsere Liefer- und Versandbedingungen

Zuschläge

- Mindermengenzuschlag
- Trockeneiszuschlag
- Gefahrgutzuschlag
- Expressversand

SZABO-SCANDIC HandelsgmbH
Quellenstraße 110, A-1100 Wien
T. +43(0)1 489 3961-0
F. +43(0)1 489 3961-7
mail@szabo-scandic.com
www.szabo-scandic.com

linkedin.com/company/szaboscandic

Order online now!
www.rockland.com
tech@rockland.com
+1 484.791.3823

Datasheet for BSA-10

Bovine Serum Albumin - Fraction V

Overview

Description:	Bovine Serum Albumin - Fraction V (Immunoglobulin and Protease Free) - BSA-10
Item No.:	BSA-10
Size:	10 g
Applications:	ELISA, FC, Functional Assay, IF, IHC, LFA, WB
Origin:	Bovine

Product Details

Background:	Bovine Serum Albumin (BSA) is used for various biochemical applications including ELISA (Enzyme-Linked Immunosorbent Assay), high content screening assays, western blotting, FACS Buffer and immunohistochemistry. BSA as a blocking reagent is particularly useful with casein-sensitive antibodies, such as phospho-specific antibodies. Also used as a nutrient in cell and microbial culture. In restriction digests, BSA is used to stabilize some enzymes during digestion of DNA and to prevent adhesion of the enzyme to reaction tubes and other vessels. Bovine Serum Albumin can also be used to determine the quantity of other proteins, by comparing an unknown quantity of protein to known amounts of BSA.
Synonyms:	Bovine serum albumin fraction V, Bovine Albumin, BSA, BSA Blocker, BSA Blocking
Species of Origin:	Bovine

Target Details

Purity/Specificity:	Purity (%): 100% by Agarose Zone electrophoresis Moisture (%) 5% Loss on Drying pH: 7.0 Ash: <2.0% Protein (%): 98% by nitrogen analysis Protease: <0.005 Units/mg Heavy Metals: (Pb) < 10 ppm by ICP Endotoxin: < 3 EU/mg by LAL IgG: Not Detected NEFA: N/A
Relevant Links:	• BSA-10 SDS

Application Details

Suggested Applications:	ELISA, FC, Functional Assay, IF, IHC, LFA, WB (Based on references)
Application Note:	Bovine Serum Albumin - Fraction V is suitable for use in lateral flow, in protease sensitive assays such as RIA, EIA and nucleic acid hybridization, use as a stabilizing agent for proteins and enzymes including dilute solutions of antibody, use as a blocking agent to reduce non-specific binding for FACS, IF, IHC, and WB.
Assay Dilutions:	All assays should be optimized by the user. Recommended dilutions (if any) may be listed below.
ELISA:	User Optimized
FC:	User Optimized
FLISA:	User Optimized
IF:	User Optimized
IHC:	User Optimized
IP:	User Optimized
WB:	User Optimized
Other:	Purity (%): 100% by Agarose Zone electrophoresis Moisture (%) 0.9 % Loss on Drying pH: 7.0 Protein (%): 100.5 % by nitrogen analysis. Protease: <0.005 Units/mg Heavy Metals: < 0.49 ppm by ICP Endotoxin: < 0.1 EU/mg by LAL

Formulation

Physical State:	Lyophilized
Buffer:	None
Preservative:	None
Stabilizer:	None

Reconstitution Buffer:	Restore with deionized water (or equivalent)

Shipping & Handling

Shipping Condition:	Ambient
Storage Condition:	Store container at 4° C prior to opening.
Expiration:	Expiration date is one (1) year from date of receipt.

Images

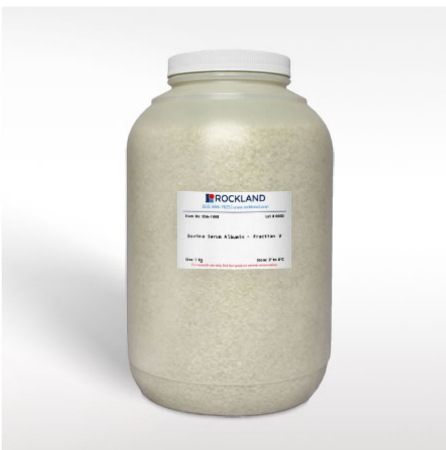

Bottle
Bovine Serum Albumin - Fraction V

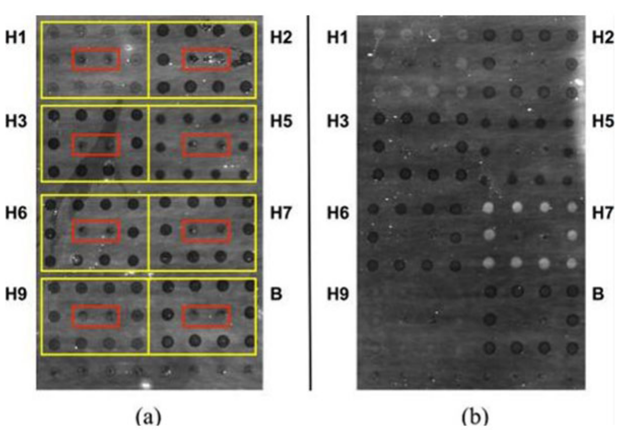

Dot Blot
Strong responses to polyclonal anti-HA antiserum are readily observable on an AIR hemagglutinin microarray.(a) 1% BSA control (p/n BSA-10). (b) Anti-H7 polyclonal antiserum (A/Netherlands/219/2003, H7N7), 1:80 dilution (1.3%) in 1% BSA. Spots showing substantially increased brightness indicate binding to immobilized H7. In both cases, antigens were arrayed in square patterns as indicated by the yellow boxes in (a); a mouse IgG Fc domain (p/n 010-0103) was included as negative control (red boxes). Slight differences in spot intensity in the control (a) are due to differences in deposition efficiency for different antigens or controls. Specific antigens used in these experiments are indicated in Table 2. Goat anti-fluorescein, (p/n 600-101-096) used as an internal negative control.
Fig 1. PMID: 26241048.

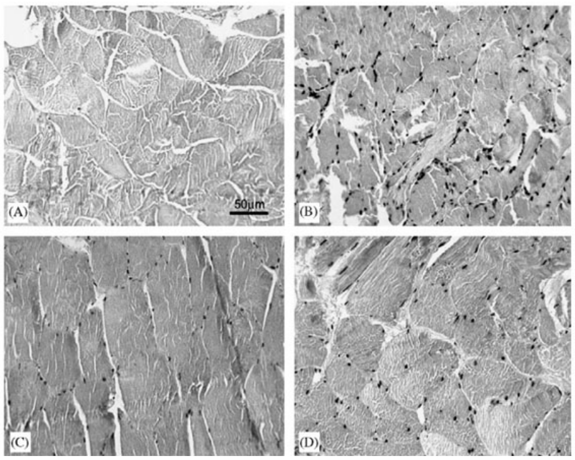

Immunohistochemistry
(I) Immunostaining for 8OhdG: (A) negative control, (B) muscle from subject 465 yr (positive control), (C) muscle from weight maintainer, and (D) muscle from weight gainer. For the 8OHdG assay, samples were treated with 10 mg/ml Proteinase K in phosphate-buffered saline (PBS) (0.05 M phosphate, 0.15 M NaCl, pH 7.4) with 1% bovine serum albumin (p/n BSA-50) for 40 min at 37 1C, and incubated in 5% skim milk in PBS for 2 h. Figure 1. PMID: 16687193.

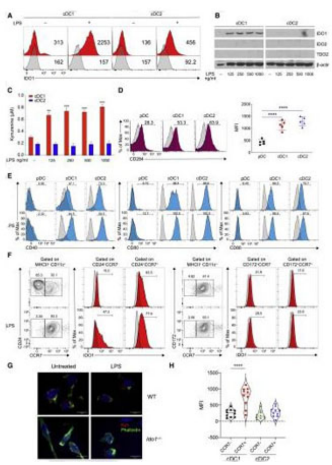

Flow Cytometry
IDO1 is selectively induced in cDC1 cells following LPS stimulation
(A) IDO1 expression was analyzed by IS in BMDCs (n = 5).
(B) Immunoblot analysis was carried out for IDO1, IDO2, TDO2, and β-actin expression (n = 3).
(C) Supernatants from cells prepared as in (B) were analyzed for l-kynurenine content by HLPC.
(D and E) Flow plot (left) and quantification (right) of CD284 (D), and flow plot of CD40, CD80, and CD86 (E) on DC subsets (n = 3).
(F) BM-derived cDC1 and cDC2 were treated as in (B) and IDO1 expression evaluated in CCR7− and CCR7+ populations treated as in (B), pre-gated on cDC1 and cDC2 (n = 3).
(G) Immunofluorescence analysis of l-kynurenine expression in sorted CCR7+ cDC1 of different genotypes treated as in (B) (n = 3).
(H) IDO1 expression (MFI) in thymic CCR7− and CCR7+ dendritic cell subsets, gated on CD11c+MHCII+XCRI +CD117− and CD11c+MCHII+CD172+CD117− (n = 3).
Data are shown as mean ±
SD. ?? $p < 0.01$, ??? $p < 0.001$, ???? $p < 0.0001$, one-way (D and H) or two-way (C) ANOVA followed by Bonferroni multiple comparison test. Isotype control as gray histogram. Figure 1. PMID: 35704993.

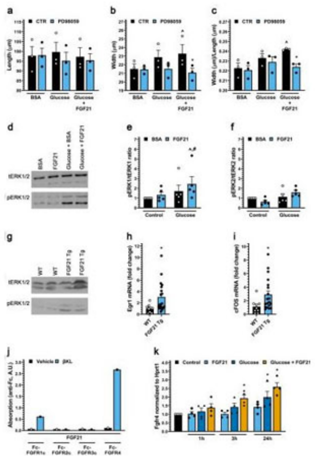

Western Blot
FGF21 activates ERK1/2 in cultured cardiac myocytes in the presence of high glucose and in heart tissue of mice. (a–c) Length, width and width to length ratio for ARVMs treated with BSA (control), FGF21 (25 ng/ml), increased glucose and/or the MEK inhibitor PD98059 (20 µM) for 48 h. Bars and colored symbols indicate average mean and means of independent experiments using different myocyte preparations, respectively. (d–f) Western blot analysis of ARVMs treated with BSA (control) or mouse recombinant FGF21 (25 ng/ml) with or without 10 mM glucose for 6 h. ERK1 is p44 and ERK2 is p42. (g) Analysis of cardiac tissue from FGF21 Tg mice and wild-type littermates at 8–12 weeks of age by Western blotting. (h, i) qRT-PCR for Egr-1 and c-Fos mRNA using total RNA from heart tissue of FGF21 Tg mice and wild-type littermates at 8–12 weeks of age. (j) Binding of 1 µg of soluble β-klotho (βKL) or PBS, 500 ng of Fc-tagged FGFR 1c, 2c, 3c, or 4 to 96-well plates coated with 200 ng of FGF21. (k) qRT-PCR for FGFR4 mRNA using total RNA isolated from ARVMs treated with BSA (control), FGF21 (25 ng/ml), and/or increased glucose (15.6 mM total). Comparison between groups was performed in form of a one-way (a–c, k) or two-way (e–f) ANOVA followed by post-hoc Tukey test or a two tailed t-test (h, i). All values are expressed as mean ± SEM. (a–c) N = 3, ^p ≤ 0.05 vs. BSA CTR, *p ≤ 0.05 vs. Glucose + FGF21 CTR; (e, f) N = 5, ^p ≤ 0.05 vs. BSA CTR, #p ≤ 0.05 vs. FGF21 CTR; (h, i) N = 9–19, *p ≤ 0.05 vs. WT; (k) N = 4, *p ≤ 0.05 vs. CTR. All Western blots are cropped, and original blots are presented in Supplementary Fig. 3. Figure 3. PMID: 35513431.

References

- Afshar-Saber W et al. ALDH5A1-deficient iPSC-derived excitatory and inhibitory neurons display cell type specific alterations. *Neurobiol Dis.* (2024)
- Helble JD et al. Single-cell RNA sequencing of murine ankle joints over time reveals distinct transcriptional changes following Borrelia burgdorferi infection. *iScience.* (2023)
- Chen W et al. The mRNA-binding protein DDX3 mediates TGF-β1 upregulation of translation and promotes pulmonary fibrosis. *JCI Insight.* (2023)
- Neira V et al. Identification and characterization of porcine Rotavirus A in Chilean swine population. *Front Vet Sci.* (2023)
- Kurosaki T et al. Integrative omics indicate FMRP sequesters mRNA from translation and deadenylation in human neuronal cells. *Mol Cell.* (2022)

- Cho H et al. AKT constitutes a signal-promoted alternative exon-junction complex that regulates nonsense-mediated mRNA decay. *Mol Cell.* (2022)
- Chio TI et al. A BODIPY-Based Probe Enables Fluorogenicity via Thiol-Dependent Modulation of Fluorophore Aggregation. *Molecules.* (2022)
- Pilling D et al. The sialidase NEU3 promotes pulmonary fibrosis in mice. *Respir Res.* (2022)
- Lee IK et al. Monitoring Therapeutic Response to Anti-FAP CAR T Cells Using [18F]AlF-FAPI-74. *Clin Cancer Res.* (2022)
- Kirolos SA et al. The extracellular sialidase NEU3 primes neutrophils. *J Leukoc Biol.* (2022)
- Christopher Yanucil et al. Soluble α-klotho and heparin modulate the pathologic cardiac actions of fibroblast growth factor 23 in chronic kidney disease. *Kidney Int.* (2022)
- Gargaro, M et al. Indoleamine 2,3-dioxygenase 1 activation in mature cDC1 promotes tolerogenic education of inflammatory cDC2 via metabolic communication. *Immunity* (2022)
- Yanucil, C et al. FGF21-FGFR4 signaling in cardiac myocytes promotes concentric cardiac hypertrophy in mouse models of diabetes. *Scientific Reports* (2022)
- Boccasavia, VL et al. Antigen presentation between T cells drives Th17 polarization under conditions of limiting antigen. *Cell Reports* (2021)
- Kurosaki, T et al. Loss of the fragile X syndrome protein FMRP results in misregulation of nonsense-mediated mRNA decay. *Nature Cell Biology* (2021)
- Rahman F et al. DYNC1LI2 regulates localization of the chaperone-mediated autophagy receptor LAMP2A and improves cellular homeostasis in cystinosis. *Autophagy.* (2021)
- Papimi D et al. The Aurora B gradient sustains kinetochore stability in anaphase. *Cell Rep.* (2021)
- Woodworth MA et al. Multiplexed single-cell profiling of chromatin states at genomic loci by expansion microscopy. *Nucleic Acids Research* (2021)
- Portillo AL et al. Production of human CAR-NK cells with lentiviral vectors and functional assessment in vitro. *STAR Protoc.* (2021)
- Ahn TS et al. Commercial immunoglobulin products contain cross-reactive but not neutralizing antibodies against SARS-CoV-2. *J Allergy Clin Immunol.* (2021)
- Burgos-Bravo F et al. Application of Force to a Syndecan-4 Containing Complex With Thy-1–αVβ3 Integrin Accelerates Neurite Retraction. *Front Mol Biosci.* (2020)
- Zhang J, et al. Diminution of Phagocytosed Micro/Nanoparticles by Tethering with Immunoregulatory CD200 Protein. *Sci Rep.* (2020)
- Zhang J, et al. Blockade of Macrophage Adhesion to CD200-treated Polystyrene Culture Surface. *J Biomed Mater Res A.* (2020)
- Porterfield V. et al. A three-dimensional dementia model reveals spontaneous cell cycle re-entry and a senescence-associated secretory phenotype. *Neurobiol Aging.* (2020)
- Mao C. et al. Feature-rich covalent stains for super-resolution and cleared tissue fluorescence microscopy. *Sci Adv.* (2020)

- Schuster-Little N, Madera S, Whelan R. Developing a mass spectrometry-based assay for the ovarian cancer biomarker CA125 (MUC16) using suspension trapping (STrap). *Anal Bioanal Chem.* (2020)
- Gronseth, E et al. Astrocytes influence medulloblastoma phenotypes and CD133 surface expression. *PloS One* (2020)
- Moreno-Olivas F et al. ZnO nanoparticles affect nutrient transport in an in vitro model of the small intestine. *Food Chem Toxicol.* (2019)
- Leung CS, Douglass SM, Morselli M, et al. H3K36 Methylation and the Chromodomain Protein Eaf3 Are Required for Proper Cotranscriptional Spliceosome Assembly. *Cell Rep.* (2019)
- Pollock SR, Schinlever AR, Rohani A, Kashatus JA, Kashatus DF. RalA and RalB relocalization to depolarized mitochondria depends on clathrin-mediated endocytosis and facilitates TBK1 activation. *PLoS One.* (2019)
- Zhang J, He J, Johnson JL, et al. Cross-regulation of defective endolysosome trafficking and enhanced autophagy through TFEB in UNC13D deficiency. *Autophagy.* (2019)
- Mondanelli G, Volpi C. Differentiation of Myeloid-derived Suppressor Cells from Murine Bone Marrow and Their Co-culture with Splenic Dendritic Cells. *Bio Protoc.* (2017)
- Allen JN, Dey A, Nissly R, et al. Isolation, Characterization, and Purification of Macrophages from Tissues Affected by Obesity-related Inflammation. *J Vis Exp.* (2017)
- Chang Q, Ornatsky O, Hedley D. Staining of Frozen and Formalin-Fixed, Paraffin-Embedded Tissues with Metal-Labeled Antibodies for Imaging Mass Cytometry Analysis. *Curr Protoc Cytom.* (2017)
- Spencer, KC et al. A three dimensional in vitro glial scar model to investigate the local strain effects from micromotion around neural implants. *Lab on a Chip* (2017)
- Domogauer JD, de Toledo SM, Azzam EI. A Mimic of the Tumor Microenvironment: A Simple Method for Generating Enriched Cell Populations and Investigating Intercellular Communication. *J Vis Exp.* (2016)
- Bucukovski, J et al. A Multiplex Label-Free Approach to Avian Influenza Surveillance and Serology. *PloS One* (2015)
- Keeler, GD et al. Effects of delayed delivery of dexamethasone-21-phosphate via subcutaneous microdialysis implants on macrophage activation in rats. *Acta Biomaterialia* (2015)
- Keeler, GD et al. Localized delivery of dexamethasone-21-phosphate via microdialysis implants in rat induces M(GC) macrophage polarization and alters CCL2 concentrations. *Acta Biomaterialia* (2015)
- Toops, KA et al. A detailed three-step protocol for live imaging of intracellular traffic in polarized primary porcine RPE monolayers. *Experimental Eye Research* (2014)
- Keeler, GD et al. Comparison of microdialysis sampling perfusion fluid components on the foreign body reaction in rat subcutaneous tissue. *European Journal of Pharmaceutical Sciences : Official Journal of the European Federation for Pharmaceutical Sciences* (2014)
- Andrew O Fung et al. Quantitative detection of PfHRP2 in saliva of malaria patients in the Philippines *Malar J.* (2012)
- Clausen TM, Christoffersen S, Dahlbäck M, et al. Structural and functional insight into how the Plasmodium falciparum VAR2CSA protein mediates binding to chondroitin sulfate A in placental malaria. *J Biol Chem.* (2012)
- Lehtinen, J et al. Pre-targeting and direct immunotargeting of liposomal drug carriers to ovarian carcinoma. *PloS One* (2012)

- Lee, Chia-Hua et al. Examining the lateral displacement of HL60 cells rolling on asymmetric P-selectin patterns. *Langmuir : the Acs Journal of Surfaces and Colloids* (2011)
- Dahlbäck M, Jørgensen LM, Nielsen MA, et al. The chondroitin sulfate A-binding site of the VAR2CSA protein involves multiple N-terminal domains. *J Biol Chem.* (2011)
- Lee CH, Bose S, Van Vliet KJ, Karp JM, Karnik R. Studying cell rolling trajectories on asymmetric receptor patterns. *J Vis Exp.* (2011)
- Makino N, Maeda T, Oyama J, et al. Antioxidant therapy attenuates myocardial telomerase activity reduction in superoxide dismutase-deficient mice. *J Mol Cell Cardiol.* (2011)
- Moorjani S, Nielson R, Chang XA, Shear JB. Dynamic remodeling of subcellular chemical gradients using a multi-directional flow device. *Lab Chip.* (2010)
- Resende M, Ditlev SB, Nielsen MA, et al. Chondroitin sulphate A (CSA)-binding of single recombinant Duffy-binding-like domains is not restricted to Plasmodium falciparum Erythrocyte Membrane Protein 1 expressed by CSA-binding parasites. *Int J Parasitol.* (2009)
- Dravid G, Hammond H, Cheng L. Culture of human embryonic stem cells on human and mouse feeder cells. *Methods Mol Biol.* (2006)
- de la Maza MP, Olivares D, Hirsch S, et al. Weight increase and overweight are associated with DNA oxidative damage in skeletal muscle. *Clin Nutr.* (2006)
- McDonald JC et al. Prototyping of microfluidic devices in poly (dimethylsiloxane) using solid-object printing. *Anal Chem.* (2002)

Disclaimer